

# Floquet Chern Insulators of Light

Li He<sup>1</sup>, Zachariah Addison<sup>1</sup>, Jicheng Jin<sup>2</sup>, Eugene J. Mele<sup>1</sup>, Steven G. Johnson<sup>3</sup>, & Bo Zhen<sup>1,\*</sup>

<sup>1</sup>*Department of Physics and Astronomy, University of Pennsylvania, Philadelphia, PA 19104, USA*

<sup>2</sup>*State Key Laboratory of Advanced Optical Communication Systems and Networks, Peking University, Beijing 100871, China*

<sup>3</sup>*Department of Mathematics, Massachusetts Institute of Technology, Cambridge, MA 02139, USA.*

**Achieving topologically-protected robust transport in optical systems has recently been of great interest<sup>1-3</sup>. Most topological photonic structures can be understood by solving the eigenvalue problem of Maxwell's equations for a static linear system<sup>1,4</sup>. Here, we extend topological phases into dynamically driven nonlinear systems and achieve a Floquet Chern insulator of light in nonlinear photonic crystals (PhCs). Specifically, we start by presenting the Floquet eigenvalue problem in driven two-dimensional PhCs and show it is necessarily non-Hermitian. We then define topological invariants associated with Floquet bands using non-Hermitian topological band theory, and show that topological band gaps with non-zero Chern number can be opened by breaking time-reversal symmetry through the driving field. Furthermore, we show that topological phase transitions between Floquet Chern insulators and normal insulators occur at synthetic Weyl points<sup>5,6</sup> in a three-dimensional parameter space consisting of two momenta and the driving frequency. Finally, we numerically demonstrate the existence of chiral edge states at the interfaces between a Floquet Chern insulator**

**and normal insulators, where the transport is non-reciprocal and uni-directional. Our work paves the way to further exploring topological phases in driven nonlinear optical systems and their optoelectronic applications, and our method of inducing Floquet topological phases is also applicable to other wave systems, such as phonons, excitons, and polaritons.**

The field of topological photonics seeks to classify and demonstrate various topological phases in Maxwell's equations, and to apply their associated robust states in optical systems. Though initially inspired by progress in electronic systems, topological photonics has recently developed in multiple directions using its unique ingredients, such as the easy incorporation of non-Hermiticity via material gain<sup>7-9</sup> or radiative loss<sup>10</sup>. Many important applications of topological photonics, such as optical isolators and circulators, are non-reciprocal in nature, which means they are exclusive for topological phases in systems with broken time-reversal symmetry. In static structures, such topological phases are often achieved by starting with engineered degeneracies between two bands of a PhC - in an either linear (Dirac) or quadratic fashion - followed by a static perturbation that breaks reciprocity, such as gyromagnetic effects<sup>11-14</sup>. The resulting systems are often referred to as Chern insulators, as their topological gaps can support uni-directional modes, whose transport is protected by the topological invariant of Chern numbers. Another important method to break reciprocity is through temporal modulation<sup>15</sup>, yet the understanding of topological phases in dynamically driven optical systems is often limited to tight-binding models of coupled resonators<sup>16,17</sup> or waveguides<sup>18,19</sup>.

Here, we study Floquet topological phases in general nonlinear PhCs under external drive

and show how non-reciprocal transport can be achieved in, what we call, a Floquet Chern insulator. We start by formulating the Floquet eigenvalue problem of Maxwell's equations, and show it is necessarily non-Hermitian but with real eigenvalues in many cases. This is different from Floquet topological phases in electronic systems, which are always defined through Hermitian eigenvalue problems. After elucidating what time-reversal symmetry ( $T$ ) entails in driven systems, we engineer the external drive to break  $T$  and to close and re-open Floquet gaps to change Chern numbers. Finally, through numerical simulations of realistic designs, we present an explicit example of a Floquet Chern insulator, along with the dispersions and locations of uni-directional chiral edge states at its interfaces with normal insulators.

We start by showing that new bandgaps - Floquet gaps - can be created in driven nonlinear PhCs, which do not exist in the static band structure. We consider a two-dimensional PhC that involves second-order optical nonlinear materials such as  $\text{LiNbO}_3$ . The static band structure is schematically shown in Fig. 1b, and we focus on two isolated bands:  $|1\rangle$  in blue and  $|2\rangle$  in red, which are separated by a gap in the spectrum. When an external driving field at frequency  $\Omega$  is applied along the normal direction, the discrete spatial translation symmetry of the system is preserved, but the continuous temporal translation symmetry is broken, leaving only a discrete temporal translation symmetry. Accordingly, each band creates copies of itself - Floquet bands - shifted up or down in the spectrum by  $m\Omega$ , where  $m$  is an integer. When  $\Omega$  is slightly larger than the static gap, two of the Floquet bands,  $|1, m = 0\rangle$  and  $|2, m = -1\rangle$ , cross, and the coupling between them  $V_{21}$  opens a new gap - Floquet gap - that is controlled by the driving field. When the driving field is weak, the size of the Floquet gap is linearly proportional to the coupling

strength  $|V_{21}|$ , meaning this gap can only be closed at momentum ( $\mathbf{k}$ ) points where the complex coupling term vanishes:  $V_{21}(\mathbf{k}) = 0$ . We later show these singular points represent the topological phase transitions between Floquet Chern insulators and normal insulators and are, fundamentally, synthetic Weyl points<sup>20,21</sup>.

Next, we present the Floquet eigenvalue problem of Maxwell's equations in this system. The result (Eq. 1) is achieved by adding time-dependent nonlinear permittivity tensor  $\bar{\epsilon}_{\text{nl}}(t)$  - determined by both the nonlinear material and the driving field - into the static eigenvalue problem<sup>1</sup>.

$$A\Psi = i\partial_t[(B_0 + B_{\text{nl}})\Psi] \quad (1a)$$

$$A = \begin{pmatrix} 0 & i\nabla \times \\ -i\nabla \times & 0 \end{pmatrix}, B_0 = \begin{pmatrix} \bar{\epsilon}_1 & 0 \\ 0 & \mu_0 \end{pmatrix}, B_{\text{nl}} = \begin{pmatrix} \bar{\epsilon}_{\text{nl}}(t) & 0 \\ 0 & 0 \end{pmatrix} \quad (1b)$$

where  $\bar{\epsilon}_1$  is the linear permittivity tensor, and  $\Psi(t) = (\mathbf{E}, \mathbf{H})^T$  are the complex electromagnetic fields. Here, we focus on instantaneous nonlinear processes and assume all materials involved are dispersion-less and loss-less for simplicity, although dispersive medium can potentially also be included<sup>22</sup>. Compared to the Floquet eigenvalue problem of Schrödinger equation<sup>23-25</sup>, our problem is different in a few unique ways. First, it is necessarily non-Hermitian, as the  $i\partial_t$  term cannot commute with the  $B_{\text{nl}}(t)$  term on the right hand side of Eq. 1a, though each individual term is Hermitian. Second, interestingly, the Floquet eigenvalues can be guaranteed as real under some conditions discussed later. We solve this Floquet eigenvalue problem by expanding the solution  $\Psi(t) = e^{i\mathbf{k}\cdot\mathbf{r}-i\varepsilon t} \sum_{jm} c_{jm} |j, m\rangle$  in the basis of Floquet states  $|j, m\rangle = |j\rangle e^{im\Omega t}$ . Here,  $\varepsilon$  is the quasi-energy;  $|j\rangle$  satisfies the static eigenvalue problem of  $e^{-i\mathbf{k}\cdot\mathbf{r}} A e^{i\mathbf{k}\cdot\mathbf{r}} |j\rangle = i\partial_t B_0 |j\rangle$  and therefore forms a complete basis of spatial modes. The detailed solution is presented in section I of the

Supplementary Information with discussions in section II.

To better illustrate some of the key concepts, we focus on an example when two bands become close to each other under driving  $\omega_2 - \omega_1 \approx \Omega$ , while both are far away from other bands. Our later calculations are not limited to the two-band model. Under a further rotating-wave approximation, the Floquet eigenvalue problem can be simplified into:

$$\begin{pmatrix} \omega_2 - \Omega & -\Omega V_{21} \\ 0 & \omega_1 \end{pmatrix} \begin{pmatrix} c_{2,-1} \\ c_{1,0} \end{pmatrix} = \varepsilon \begin{pmatrix} 1 & V_{21} \\ V_{21}^* & 1 \end{pmatrix} \begin{pmatrix} c_{2,-1} \\ c_{1,0} \end{pmatrix}. \quad (2)$$

As shown, this generalized eigenvalue problem is indeed non-Hermitian, but its eigenvalues can be guaranteed as real under some conditions. For example, when the driving field is exactly on-resonance, namely  $\omega_2 = \omega_1 + \Omega$ , the two Floquet eigenvalues can be further simplified as:  $\varepsilon_{\pm} = \omega_1 \pm 2|V_{21}|\sqrt{\omega_1\omega_2}$ . Both eigenvalues are necessarily real as long as we are coupling bands both at positive (or negative) frequencies ( $\omega_1\omega_2 > 0$ ). Physically, these scenarios are analogous to the depletable sum-frequency generation: power oscillates between a depletable pump  $\omega_2$  and the sum-frequency beam  $\omega_1$ , but their total photon number remains fixed in time<sup>26</sup>. On the other hand, complex eigenvalues may appear when a positive-frequency mode is coupled to a negative-frequency mode ( $\omega_1\omega_2 < 0$ ) and the resulting Floquet modes may grow exponentially in time. These scenarios are analogous to optical parametric amplification where a non-depletable pump beam ( $|\omega_1| + |\omega_2|$ ) amplifies the signal and idler beams<sup>26</sup>. In this Letter, we focus on the first situation where Floquet eigenvalues are real. Topological phase transitions can only happen at  $\mathbf{k}$  points where the gap is closed, requiring the coupling term  $V_{21} = 0$ . This is equivalent to requiring the complex phase  $\arg V_{21}$  to be undefined, or to be a topological defect<sup>27</sup>, in  $\mathbf{k}$  space.

Next, we show how such topological defects can be synthesized by engineering the polarization of the driving field. Our considered PhC sample is shown in Fig. 2a, which is consisted of a hexagonal lattice, with lattice constant  $a$ , of regions made of silicon ( $\epsilon = 12.25$ ) and regions made of  $z$ -cut LiNbO<sub>3</sub> ( $\epsilon_{xx} = \epsilon_{yy} = 4.97$ ,  $\epsilon_{zz} = 4.67$ ). Both inversion and rotation symmetries are broken to lift all degeneracies at high-symmetry  $\mathbf{k}$  points. The static band structure is calculated using Finite Element Methods (see Methods for details) and shown in Fig. 2b. In the static structure, TE bands ( $H_z, E_x, E_y$ ; red) are decoupled from the TM bands ( $E_z, H_x, H_y$ ; blue), due to the mirror symmetry in the  $z$  direction. However, under a driving field polarized in the  $xy$  plane, TE and TM bands are coupled: specifically, the external field  $E_{x,y}^d$  drives the second-order optical nonlinearity of LiNbO<sub>3</sub>,  $\chi_{zxx}^{(2)}$  and  $\chi_{zyy}^{(2)}$ , and creates  $\epsilon_{xz,zx}$  and  $\epsilon_{yz,zy}$  terms in the effective permittivity tensor of LiNbO<sub>3</sub>. These four terms break the mirror symmetry in  $z$  and couple the  $E_z$  component of a TM mode (blue) to the  $E_{x,y}$  components of a TE mode (red). By analyzing the nonlinear optical property of LiNbO<sub>3</sub>, one can show only TE-TM bands are coupled via modulation in this setup, while the Floquet TE-TE or TM-TM bands will not couple to each other (see Methods for details).

We found that time-reversal symmetry ( $T$ ) in the Floquet eigenvalue problem is defined as  $V_{21}(\mathbf{k}) = V_{21}^*(-\mathbf{k})$ . Furthermore, we found  $T$  is preserved when the driving field is linearly polarized and no topological Floquet gap can be opened. On the other hand, elliptically-polarized driving fields break  $T$ . The condition on  $T$  in these two scenarios can be intuitively understood by analyzing the temporal evolution of the instantaneous optical principle axes of LiNbO<sub>3</sub>: under a linearly polarized monochromatic drive, one optical axis remains static, while the other two oscillate in a time-reversal invariant manner. In comparison, under an elliptically polarized drive,

all three optical axes rotate around the  $z$  axis at the driving frequency and this spinning behavior breaks  $T$ . See section IV and V of the Supplementary Information for more details.

The properties associated with time-reversal symmetry are confirmed in our simulation results of the modal coupling terms  $V_{21}$  as shown in Fig. 2c,d. Specifically, under a linearly polarized drive ( $T$ -symmetric),  $V_{21}$  reduces to 0 at two opposite  $\mathbf{k}$  points, shown as two bright spots in Fig. 2c. Furthermore, these two topological defects carry opposite topological charges  $q$ , which are defined through the winding numbers of the complex phase:

$$q = \frac{1}{2\pi} \oint_C d\mathbf{k} \cdot \nabla_{\mathbf{k}} \arg V_{21}. \quad (3)$$

Here  $C$  is a closed path in  $\mathbf{k}$  space that encircles the defect in the counter-clockwise direction. Consequently, the Floquet gap can be closed and re-opened by tuning the driving frequency; however, the transition always happens at a pair of opposite  $\mathbf{k}$  points and the Floquet bands are always topologically trivial in  $T$ -symmetric cases. See section VI of the Supplementary Information for results of the Floquet band structures, and section VII for the definition of Berry curvature and Chern number of Floquet bands. On the other hand, under an elliptically polarized drive ( $T$ -broken), topological defects appear without any symmetry (Fig. 2d). As a result, the Floquet gap can close and re-open at a single  $\mathbf{k}$  point, as  $V_{21}(\mathbf{k})$  is no longer related to  $V_{21}(-\mathbf{k})$ . In our system, this topological phase transition happens at  $\Omega_2 a / 2\pi c = 0.366$  (middle gray circle) when modulation frequency reduces from  $\Omega_1 a / 2\pi c = 0.382$  (innermost circle) to  $\Omega_3 a / 2\pi c = 0.35$  (outermost circle).

Next, we study topological phase transitions between Floquet Chern insulators and normal

insulators and show these transition points are synthetic Weyl points in the parameter space of  $(k_x, k_y, \Omega)$  as shown in Fig. 3a. First, the Floquet band gap closes at the transition point, but grows linearly as  $\Omega$  deviates from  $\Omega_2$  (Fig. 3b). Furthermore, we compare the Floquet spectra near the transition point: the bands are gapped when either  $\Omega > \Omega_2$  (top panel of Fig. 3c) or  $\Omega < \Omega_2$  (bottom); however, the two Floquet bands touch at a singular point in  $k$  space in a linear fashion when  $\Omega = \Omega_2$  (middle). As the gap size grows linearly as the system parameter deviates from a single point in the three-dimensional parameter space of  $(k_x, k_y, \Omega)$ , this transition point is a Weyl point. We further track the Chern numbers of the Floquet bands as  $\Omega$  is varied: the Chern number of the top (bottom) band changes by 1 (-1) as  $\Omega$  scans through  $\Omega_2$  (Fig. 3d), which confirms our Weyl point claim. Additionally, the Chern numbers of the two bands jump in opposite directions with their sum fixed at 0, which confirms our system is a Chern insulator.

Finally, we show the existence of chiral edge states at the interfaces between a Floquet Chern insulator (gray region in Fig. 4a) with normal insulators (white region). In this super-cell geometry, we apply periodic boundary conditions in both  $x$  and  $y$  directions, and these two insulators have two interfaces, top and bottom. The topological region shares the same setup as the bottom panel of Fig. 3c; the trivial region is driven at the same frequency  $\Omega_3 a / 2\pi c = 0.35$ , but with a linearly polarized light  $(2\hat{x} + \hat{y})$  that preserves  $T$ . Through a super-cell calculation (see section VIII of Supplementary Information for details), all bands in the system are computed. Aside from the bulk bands in the non-trivial region and trivial regions, we see chiral edge states (red and blue lines) emerge at the two interfaces with frequencies going across the topological band gap. Their mode profiles further confirm these are indeed edge states localized at the top (red) and bottom



(blue) interfaces (Fig. 4c); in comparison, a bulk mode (black) is delocalized along the  $y$ -direction. Although helical spatial modulation of waveguide arrays achieve Floquet Chern insulators in the transverse plane<sup>18</sup>, our approach breaks reciprocity for the system as a whole and thus enables optical isolation through the chiral edge states. The number of edge states and their travelling directions are consistent with the Floquet topological band theory results for electronic systems<sup>28</sup>.

To sum up, we present a general scheme to achieve Floquet topological phases in nonlinear photonic crystals defined by the Floquet eigenvalue problems in Maxwell's equations. We show that Floquet band gaps can be closed and re-opened in a virtually arbitrary fashion by engineering the driving field (polarization and frequency). Using this scheme, we propose and numerically demonstrate a Floquet Chern insulator of light by breaking time-reversal symmetry using elliptically polarized driving fields. We show the Floquet topological phase transitions are synthetic Weyl points. Finally, we numerically demonstrate the existence of chiral edge states at the interfaces between topologically trivial and non-trivial regions. Our work paves the way to further classifying and realizing topological phases in dynamically driven optical systems and their optoelectronic applications in communication and signal routing.

Note added: During the completion of this work, we became aware of a related study by Fang and Wang<sup>29</sup>.

## Methods

**Numerical simulation of Maxwell equation using Finite Element Methods.** The band structures and mode profiles are calculated using Finite Element Methods in COMSOL Multiphysics 5.3a. Specifically, we first compute the static band structures and mode profiles using the linear permittivity in a 2D geometry with periodic boundary conditions. The modal overlaps  $V_{21}(\mathbf{k})$  are calculated by taking the inner product between the two modes mediated by external drive and nonlinear susceptibility of the LiNbO<sub>3</sub>. Finally, we input these coupling terms into the master equation (Eq. S1 in the supplementary information) to calculate the eigenvalues, mode profiles, Berry curvatures, and Chern numbers of the Floquet bands.

**Band coupling via the second-order optical nonlinearity of LiNbO<sub>3</sub>.** Under an driving field polarized in the  $xy$  plane, TE-TM bands are coupled to each other through  $\chi_{zxx}^{(2)}$  ( $d_{31}$ ) and  $\chi_{zyy}^{(2)}$  ( $d_{32}$ ) terms of LiNbO<sub>3</sub>, both of which are 5 pm/V<sup>30</sup>. On the other hand, the  $E_z$  components of TM modes cannot couple to each other via modulation, because the relevant terms,  $\chi_{zzz}^{(2)}$  and  $\chi_{zyz}^{(2)}$ , are both 0 in LiNbO<sub>3</sub>. Similarly, the  $E_{x,y}$  components of TE modes cannot couple via modulation either.

1. Lu, L., Joannopoulos, J. D. & Soljačić, M. Topological photonics. *Nature Photonics* **8**, 821 (2014).
2. Khanikaev, A. B. & Shvets, G. Two-dimensional topological photonics. *Nature Photonics* **11**, 763 (2017).

3. Ozawa, T. *et al.* Topological photonics. *arXiv preprint arXiv:1802.04173* (2018).
4. Noh, J. *et al.* Experimental observation of optical weyl points and fermi arc-like surface states. *Nature Physics* **13**, 611 (2017).
5. Lu, L. *et al.* Experimental observation of weyl points. *Science* **349**, 622–624 (2015).
6. Armitage, N., Mele, E. & Vishwanath, A. Weyl and dirac semimetals in three-dimensional solids. *Reviews of Modern Physics* **90**, 015001 (2018).
7. Bandres, M. A. *et al.* Topological insulator laser: Experiments. *Science* **359**, eaar4005 (2018).
8. Bahari, B. *et al.* Nonreciprocal lasing in topological cavities of arbitrary geometries. *Science* **358**, 636–640 (2017).
9. Peano, V., Houde, M., Marquardt, F. & Clerk, A. A. Topological quantum fluctuations and traveling wave amplifiers. *Physical Review X* **6**, 041026 (2016).
10. Zhou, H. *et al.* Observation of bulk fermi arc and polarization half charge from paired exceptional points. *Science* **359**, 1009–1012 (2018).
11. Wang, Z., Chong, Y., Joannopoulos, J. D. & Soljačić, M. Reflection-free one-way edge modes in a gyromagnetic photonic crystal. *Physical review letters* **100**, 013905 (2008).
12. Wang, Z., Chong, Y., Joannopoulos, J. D. & Soljačić, M. Observation of unidirectional backscattering-immune topological electromagnetic states. *Nature* **461**, 772 (2009).
13. Haldane, F. & Raghu, S. Possible realization of directional optical waveguides in photonic crystals with broken time-reversal symmetry. *Physical review letters* **100**, 013904 (2008).

14. Skirlo, S. A. *et al.* Experimental observation of large Chern numbers in photonic crystals. *Physical review letters* **115**, 253901 (2015).
15. Jalas, D. *et al.* What is and what is not an optical isolator. *Nature Photonics* **7**, 579 (2013).
16. Yuan, L. & Fan, S. Bloch oscillation and unidirectional translation of frequency in a dynamically modulated ring resonator. *Optica* **3**, 1014–1018 (2016).
17. Lin, Q., Sun, X.-Q., Xiao, M., Zhang, S.-C. & Fan, S. A three-dimensional photonic topological insulator using a two-dimensional ring resonator lattice with a synthetic frequency dimension. *Science Advances* **4**, eaat2774 (2018).
18. Rechtsman, M. C. *et al.* Photonic Floquet topological insulators. *Nature* **496**, 196 (2013).
19. Maczewsky, L. J., Zeuner, J. M., Nolte, S. & Szameit, A. Observation of photonic anomalous Floquet topological insulators. *Nature communications* **8**, 13756 (2017).
20. Lin, Q., Xiao, M., Yuan, L. & Fan, S. Photonic Weyl point in a two-dimensional resonator lattice with a synthetic frequency dimension. *Nature communications* **7**, 13731 (2016).
21. Wang, Q., Xiao, M., Liu, H., Zhu, S. & Chan, C. T. Optical interface states protected by synthetic Weyl points. *Physical Review X* **7**, 031032 (2017).
22. Raman, A. & Fan, S. Photonic band structure of dispersive metamaterials formulated as a Hermitian eigenvalue problem. *Physical review letters* **104**, 087401 (2010).
23. Lindner, N. H., Refael, G. & Galitski, V. Floquet topological insulator in semiconductor quantum wells. *Nature Physics* **7**, 490 (2011).

24. Dittrich, T. *et al.* *Quantum transport and dissipation*, vol. 3 (Wiley-Vch Weinheim, 1998).
25. DAlessio, L. & Rigol, M. Dynamical preparation of floquet chern insulators. *Nature communications* **6**, 8336 (2015).
26. Boyd, R. W. *Nonlinear optics* (Elsevier, 2003).
27. Mermin, N. D. The topological theory of defects in ordered media. *Reviews of Modern Physics* **51**, 591 (1979).
28. Rudner, M. S., Lindner, N. H., Berg, E. & Levin, M. Anomalous edge states and the bulk-edge correspondence for periodically driven two-dimensional systems. *Physical Review X* **3**, 031005 (2013).
29. Fang, K. & Wang, Y. Anomalous quantum Hall effect of light in Bloch-wave modulated photonic crystals. *arXiv:1902.02887 [cond-mat, physics:physics]* (2019). ArXiv: 1902.02887.
30. Sutherland, R. L. *Handbook of nonlinear optics* (CRC press, 2003).

**Acknowledgements** We thank H. Zhou for discussions. LH was supported by NSF through the University of Pennsylvania Materials Research Science and Engineering Center DMR-1720530 and grant DMR-1838412. Work by ZA and EJM interpreting the topological character of Floquet states was supported by DOE Office of Basic Energy Sciences under grant DE FG 02 ER84-45118. SGJ was supported by U.S. Army Research Office through the Institute for Soldier Nanotechnologies (W911NF-13-D- 0001). BZ was supported by the Air Force Office of Scientific Research under award number FA9550-18-1-0133.

**Author contributions** L.H and B.Z conceived the idea. L.H. carried out numerical simulations and all authors discussed and interpreted the results. L.H and B.Z. wrote the manuscript with contribution from all authors. B.Z. supervised the project.

**Competing Interests** The authors declare no competing financial interests.

**Correspondence** Correspondence and requests for materials should be addressed to Bo Zhen. (email: bozhen@sas.upenn.edu).

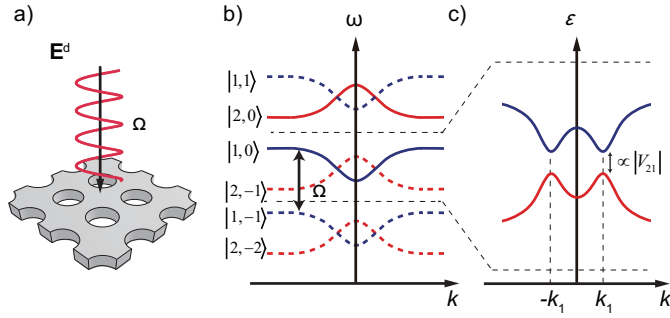


Figure 1: | **Floquet bands and gaps in a periodically driven nonlinear photonic crystal.** **a**, Schematic of a nonlinear photonic crystal (PhC) placed in a monochromatic driving field  $\mathbf{E}^d$  at frequency  $\Omega$ . **b**, Due to the periodic drive, static bands of the PhC (solid lines) create copies of themselves - Floquet bands (dashed lines) - by shifting up or down in the spectrum. **c**, Two of the Floquet bands  $|1, m = 0\rangle$  and  $|2, m = -1\rangle$  cross at  $\pm k_1$ . Their coupling term  $V_{21}$  opens a new gap  $E_g$  - Floquet gap - and its size is linearly proportional to the magnitude of their coupling strength  $|V_{21}|$  under weak drive.

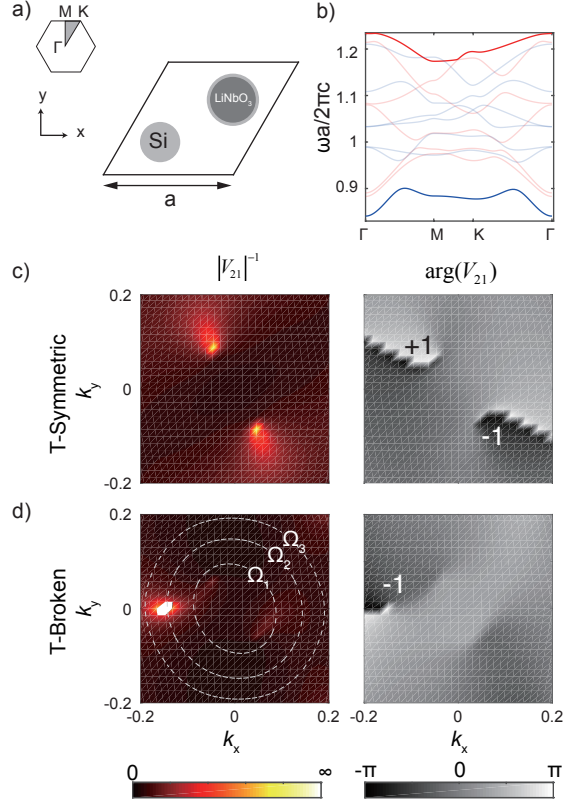


Figure 2: | **Topological charges in modal coupling terms and the influence of time-reversal symmetry.** **a**, Nonlinear PhC unit cell involving Si and  $z$ -cut LiNbO<sub>3</sub>. **b**, Static modes are separated into TE (red) and TM (blue) bands. Under a driving field polarized in the  $xy$  plane, a TE band is coupled to a TM band through  $\chi^{(2)}$  of LiNbO<sub>3</sub>. Their coupling term  $V_{21}$  is controlled by the polarization of the drive. **c**, Under a linearly-polarized drive ( $2\hat{x} + \hat{y}$ ), a pair of vortices with opposite topological charges ( $\pm 1$ ) are found in the complex phase  $\arg V_{21}$ , located at opposite  $k$  points. At these  $k$  points, the modal coupling term vanishes and  $1/|V_{21}| \rightarrow \infty$ . **d**, Under an elliptically polarized drive,  $\hat{x} - (0.32 - 4.04i)\hat{y}$ , vortices in  $\arg V_{21}$  appear without any symmetry. Topological phase transition is achieved between a Floquet normal insulator ( $\Omega = \Omega_1$ , innermost circle) and a Floquet Chern insulator ( $\Omega_3$ , outermost circle) through a single topological charge at  $\Omega_2$  (middle circle).



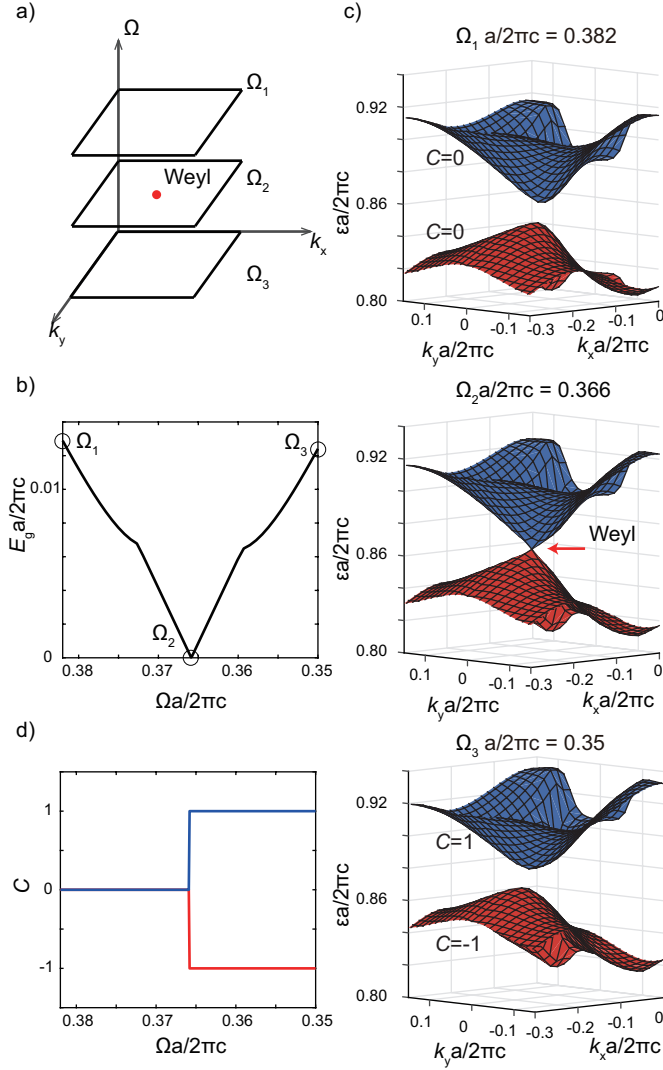


Figure 3: | **Topological phase transition points as synthetic Weyl points.** **a**, The topological phase transition point is a Weyl point in the parameter space of  $(k_x, k_y, \Omega)$ . **b**, The Floquet band gap closes at  $\Omega_2 a/2\pi c = 0.366$ , and increases linearly in its vicinity on both sides. **c**, The Floquet band structure shows a linear touching between the top and bottom bands at a singular  $\mathbf{k}$  point at  $\Omega_2$  (middle panel). This synthetic Weyl point represents a topological phase transition between a Floquet normal insulator ( $\Omega_1$ , top) and a Floquet Chern insulator ( $\Omega_3$ , bottom). **d**, The Chern numbers of the top (blue) and bottom band (red) change by 1 as  $\Omega$  scans through  $\Omega_2$ .

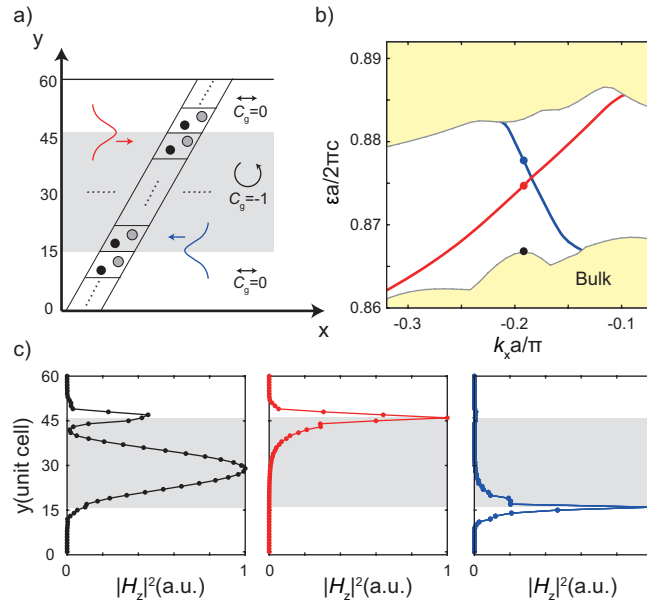


Figure 4: | **Characterizations of chiral edge states at the interfaces between a Floquet Chern insulator and normal insulators.** **a**, Schematic of the super-cell geometry with a Floquet Chern insulator placed in between two Floquet normal insulators. The Floquet Chern insulator is the same setup as the bottom panel of Fig. 3c, and all regions are driven at the same frequency  $\Omega_3$ , hence the associated gap Chern number  $C_g = -1$ . Further details of the super-cell setup can be found in section VI of the Supplementary Information. **b**, The dispersion along  $k_x$  axis shows two types of modes: bulk bands in the normal and Chern insulator regions (yellow) and uni-directional chiral edge states at the top and bottom interfaces (red and blue). **c**, Comparison among the mode profiles of a bulk state (black), the chiral edge states localized at the top interface travelling to the right (red) and at the bottom interface travelling to the left (blue).